

## Research Paper

## A PCG Implementation of an Elliptic Kernel in an Ocean Global Circulation Model Based on GPU Libraries

S. Cuomo<sup>a\*</sup>, P. De Michele<sup>a</sup> and R. Farina<sup>b</sup> and M. Chinnici<sup>c</sup>

<sup>a</sup>University of Naples “Federico II” - Dept. of Mathematics and Applications  
“R. Caccioppoli” - Via Cinthia, 80126, Naples, Italy; <sup>b</sup>CMCC, Research Center, Via  
Aldo Moro 44 (Bologna), Italy <sup>c</sup>ENEA-UTICT, Casaccia Research Center, S. Maria di  
Galeria (Roma), Italy

(released October 2012)

In this paper an inverse preconditioner for the numerical solution of an elliptic Laplace problem of a global circulation ocean model is presented. The inverse preconditioning technique is adopted in order to efficiently compute the numerical solution of the elliptic kernel by using the Conjugate Gradient (CG) method. We show how the performance and the rate of convergence of the solver are linked to the discretized grid resolution and to the Laplace coefficients of the oceanic model. Finally, we describe an easy-to-implement version of the solver on the Graphical Processing Units (GPUs) by means of scientific computing libraries and we discuss its performance.

**Keywords:** Ocean Modelling; Preconditioning Technique; GPU Programming; Scientific Computing.

**AMS Subject Classification:** 65Y5; 65Y10; 65F08; 65F35; 37N10.

## 1. Introduction

The ocean is now well known to play a dominant role in the climate system because it can initiate and amplify climate change on many different time scales. Hence, the simulation of ocean model is became a relevant but highly complex task and it involves an intricate interaction of theoretical insight, data handling and numerical modelling. Over the past several years, ocean numerical models have become quite realistic as a result of improved methods, faster computers, and global data sets. Models now treat basin-scale to global domains while retaining the fine spatial scales that are important for modelling the transport of heat, salt, and other properties over vast distances. Currently, there are many models and methods employed in the rapidly advancing field of numerical ocean circulation modelling as Nemo, Hops, MOM, POP et al (see [2] for a nice review). However, several of these numerical models are not yet optimized by using scientific computing libraries and “ad hoc” preconditioning techniques. In all these frameworks the numerical kernel is represented by the discretization of the Navier-Stokes equations [4] on a three dimensional grid and by the computation of the evolution time of each variable

---

\*Corresponding author. Email: salvatore.cuomo@unina.it

for each grid point. The high resolution computational grid requires efficient preconditioning techniques for improving the accuracy in the computed solution and parallelization strategies for answering to the huge amount of computational demand.

In this paper we propose a new solver based on preconditioned conjugate gradient (PCG) method with an approximate inverse preconditioner AINV [7] for the numerical solution of the elliptic sea-surface equation in NEMO-OPA ocean model [3], a state of the art modelling framework in the oceanographic research. The PCG is a widely used iterative method for solving linear systems with symmetric, positive definite matrix and it has proven its efficiency and robustness in a lot of applications. The preconditioning is often a bottleneck in solving the linear systems efficiently and it is well established that a suitable preconditioner increases the performance of an application dramatically.

The elliptic sea-surface equation is originally solved in NEMO-OPA by means of the PCG with diagonal preconditioner, and in our work we prove that it is inefficient and inaccurate. We build a new inverse preconditioner and we implement the PCG on a Graphic Processor Unit (GPU) by means of the linear algebra Scientific Computing libraries. The GPUs are massively parallel architectures that efficiently work with the linear algebra operations and give impressive performance improvements. They require a deep understanding of the underlying computing architecture and the programming with these devices involves a massive re-thinking of existing CPU based applications. A challenge is how to optimally use the GPU hardware adopting adequate programming techniques, models, languages and tools. In this paper, we present an easy-to-implement version of the elliptic solver with the scientific computing libraries on Compute Unified Device Architecture (CUDA) [15]. We implement a code by using CUDA based supported libraries CUBLAS [16] and CUSPARSE [17] for the sparse linear algebra and the graph computations. The library GPU based approach allows a short code development times and an easy to use GPUs implementations that can fruitfully speed up the expensive numerical kernel of an oceanographic simulator. The paper is set out as follows. In section 2 we briefly review the mathematical model: elliptic equations that are at the heart of the model. In section 3, the preconditioned conjugate gradient method used to invert the elliptic equations are described. In section 4, we outline a implementation strategy for solving the elliptic solver by using standard libraries and in section 5 we discuss the mapping of our algorithm onto a massively parallel machine. Finally, the conclusions are drawn.

## 2. The Mathematical Model

Building and running ocean models able to simulate the world of global circulation with great realism require a variety of scientific skills. In modelling the general ocean circulation it is necessary to solve problems of elliptic nature. These problems are difficult to solve, with the following issues causing the most trouble in practice[2]:

- (1) In simulations with complicated geometry (e.g., multiple islands), topography, time varying surface forcing, and many space-time scales of variability (i.e., the World Ocean), achieving a good first guess for the iterative elliptic solver is often quite difficult to achieve. This makes it difficult for elliptic solvers to converge to a solution within a reasonable number of iterations. For this reason, many climate modellers limit the number of elliptic solver iterations used, even if the solver has not converged. This approach is very

unsatisfying.

- (2) Many elliptic solvers with their associated non-local and time dependent boundary conditions (be they Neumann or Dirichlet) do not project well onto parallel distributed computers, which acts to hinder their scaling properties [23–25].

In the OPA-NEMO numerical code the primitive equations are discretized within sea-surface hypothesis [1] and the model is characterized by the three-dimensional distribution of currents, potential temperature, salinity, pressure and density [4]. The numerical method OPA-NEMO is grounded on discretizing of the primitive equation - by the use of finite differences on a three dimensional grid - and computing the time evolution to each variable "ocean" at each grid point for the entire globe [6]. A sketch of the OPA-NEMO computational model, see Figure 1, shows the complex dynamic processes that mimic the ocean circulation model, composed by steps that are many time simulated.

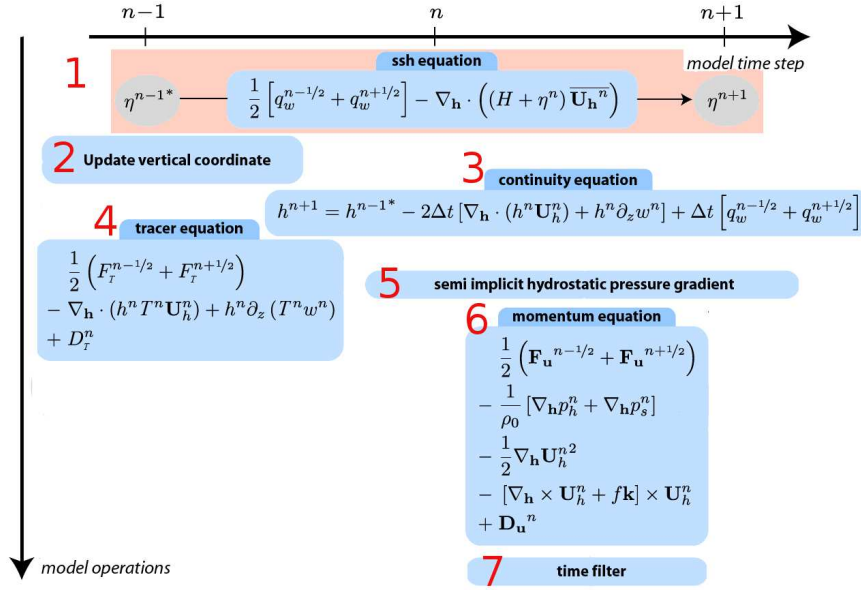


Figure 1. NEMO-OPA model.

The kernel algorithm (highlighted with red color, equation 1) solves the sea-surface height equation  $\eta$ . The elliptic kernel is discretized with semi-discrete equations, as following:

$$\eta^{n+1} = \eta^{n-1} - 2\Delta t D^n \quad (1)$$

$$2\Delta t g T_c \Delta_h D^{n+1} = D^{n+1} - D^{n-1} + 2\Delta t g \Delta_h \eta^n \quad (2)$$

$$\Delta_h = \nabla[(H + \eta^n) \nabla]. \quad (3)$$

where  $\eta^n$ ,  $n \in \mathbb{N}$  is the sea-surface height at the  $n$ -th step of the model, which describes the shape of the air-sea interface,  $D^n$  is the centered difference approximation of the first time derivative of  $\eta$ ,  $\Delta t$  is the time stepping,  $g$  is the gravity constant,  $T_c$  is a physical parameter,  $\Delta_h$  is the horizontal Laplacian operator and  $H$  is the depth of the ocean bottom [3]. Whereas the domain of the ocean models is the Earth sphere (or part of it) the model uses the geographical coordinates system  $(\lambda, \phi, r)$  in which a position is defined by the latitude  $\phi$ , the longitude  $\lambda$  and the distance from the center of the earth  $r = a + z(k)$  where  $a$  is the Earth's radius and

z the altitude above a reference sea level. The local deformation of the curvilinear geographical coordinate system is given by  $e_1, e_2$  and  $e_3$ :

$$e_1 = r \cos \phi, \quad e_2 = r, \quad e_3 = 1. \quad (4)$$

The Laplacian Operator in spherical coordinates  $\Delta_h D^{n+1}$  in (2) becomes:

$$\Delta_h D^{n+1} = \frac{1}{e_1 e_2} \left[ \frac{\partial}{\partial i} \left( \alpha(\phi) \frac{\partial D^{n+1}}{\partial i} \right) + \frac{\partial}{\partial j} \left( \beta(\phi) \frac{\partial D^{n+1}}{\partial j} \right) \right] \quad (5)$$

where:

$$\alpha(\phi) = (H + \eta^n) e_2 / e_1 \quad (6)$$

$$\beta(\phi) = (H + \eta^n) e_1 / e_2 \quad (7)$$

For the functions  $\alpha(\phi)$  in (6) and  $\beta(\phi)$  in (7), we have the following relations:

$$\lim_{\phi \rightarrow \pm \frac{\pi}{2}} \alpha(\phi) = +\infty \quad \wedge \quad \lim_{\phi \rightarrow \pm \frac{\pi}{2}} \beta(\phi) = 0 \quad (8)$$

From (8), if we choose  $M, \epsilon \in \mathbb{R}$  with  $M \gg \epsilon$  then exists an interval  $[\frac{\pi}{2} - \delta, \frac{\pi}{2}]$  or  $[-\frac{\pi}{2}, -\frac{\pi}{2} + \delta]$ , such that the following inequality holds:

$$\alpha(\phi) > M \gg \epsilon > \beta(\phi) \quad (9)$$

In physical terms, in the proximity of the geographical poles,  $(\lambda, \pm \phi/2, r)$ , there are several orders of magnitude between the functions  $\alpha(\phi)$  and  $\beta(\phi)$

The result (9), will significantly influence the rate of convergence in the iterative solver.

### 3. Inverse Preconditioned Techniques in the Elliptic Solver of the Ocean Model

Let us now consider the elliptic NEMO model [3] defined by the following coefficients:

$$\begin{aligned} C_{i,j}^{NS} &= 2\Delta t^2 H(i, j) e_1(i, j) / e_2(i, j), & C_{i,j}^{EW} &= 2\Delta t^2 H(i, j) e_2(i, j) / e_1(i, j) \\ b_{i,j} &= \delta_i(e_2 M_u) - \delta_j(e_1 M_v) \end{aligned} \quad (10)$$

where  $\delta_i$  and  $\delta_j$  are the discrete derivative operators along the axes  $\mathbf{i}$  and  $\mathbf{j}$ . The discretization of the equation (2) by means of a five-point finite difference method gives:

$$\begin{aligned} C_{i,j}^{NS} D_{i-1,j} + C_{i,j}^{EW} D_{i,j-1} - (C_{i+1,j}^{NS} + C_{i,j+1}^{EW} + C_{i,j}^{NS} + C_{i,j}^{EW}) D_{i,j} + \\ + C_{i,j+1}^{EW} D_{i,j+1} + C_{i+1,j}^{NS} D_{i+1,j} = b_{i,j}. \end{aligned} \quad (11)$$

where the equation (11) is a symmetric system of linear equations. All the elements of the sparse matrix  $\mathbf{A}$  vanish except those of five diagonals. With the natural

ordering of the grid points (i.e. from west to east and from south to north), the structure of  $\mathbf{A}$  is a block-tridiagonal with tridiagonal or diagonal blocks. The matrix  $\mathbf{A}$  is a positive-definite symmetric matrix with  $n = jpi \times jpi$  size, where  $jpi$  and  $jpi$  are respectively the horizontal dimensions of the grid discretization of the domain. The Conjugate Gradient Method is a very efficient iterative method for solving the linear system (11) and it provides the exact solution in a number of iterations equal to the size of the matrix. The convergence rate is faster as the matrix is closer to the identity one. By spectral point of view a convergence relation between the solution of the linear system and its approximation  $x_m$  is given by:

$$\|\mathbf{x} - \mathbf{x}_m\|_A < 2 \left( \frac{\sqrt{\mu_2(A)} - 1}{\sqrt{\mu_2(A)} + 1} \right)^{m-1} \|\mathbf{x} - \mathbf{x}_0\|_A \quad (12)$$

with  $\mu_2(A) = \lambda_{max}/\lambda_{min}$ , where  $\lambda_{max}$  and  $\lambda_{min}$  are respectively the greatest and the lowest eigenvalue of  $\mathbf{A}$ , and  $\|\cdot\|_A$  is the A-norm. The preconditioning framework consists to introduce a matrix  $\mathbf{M}$ , that is an approximation of  $\mathbf{A}$  easier to invert, and to solve the equivalent linear system:

$$\mathbf{M}^{-1} \mathbf{A} \mathbf{x} = \mathbf{M}^{-1} \mathbf{b} \quad (13)$$

The ocean global model NEMO-OPA uses the diagonal preconditioner, where  $\mathbf{M}$  is chosen to the diagonal of  $\mathbf{A}$ . Let us introduce the following cardinal coefficients:

$$\alpha_{i,j}^E = C_{i,j+1}^{EW} / d_{i,j} \quad \alpha_{i,j}^W = C_{i,j}^{EW} / d_{i,j} \quad (14)$$

$$\beta_{i,j}^S = C_{i,j}^{NS} / d_{i,j} \quad \beta_{i,j}^N = C_{i+1,j}^{NS} / d_{i,j} \quad (15)$$

where  $d_{i,j} = (C_{i+1,j}^{NS} + C_{i,j+1}^{EW} + C_{i,j}^{NS} + C_{i,j}^{EW})$  represents the diagonal of the matrix  $\mathbf{A}$ . The (11), using the diagonal preconditioner, can be written as:

$$-\beta_{i,j}^S D_{i-1,j} - \alpha_{i,j}^W D_{i,j-1} + D_{i,j} - \alpha_{i,j}^E D_{i,j+1} + -\beta_{i,j}^N D_{i+1,j} = \bar{b}_{i,j}. \quad (16)$$

with  $\bar{b}_{i,j} = -b_{i,j}/d_{i,j}$ .

Starting from the observations (8) and (9) we proof that the diagonal preconditioner does not work very well in some critical physical situations involving curvilinear spherical coordinates.

**PROPOSITION 3.1** *In the geographical coordinate, if  $\phi \rightarrow +\frac{\pi}{2}^-$ ,  $\Delta\lambda \rightarrow 0$ ,  $\Delta\phi \rightarrow 0$  then the conditioning number  $\mu(\mathbf{M}^{-1}\mathbf{A})$  goes to  $+\infty$ .*

**Proof.** In the geographical coordinate, i.e. when  $(i, j) \rightarrow (\lambda, \phi)$  and  $(e_1, e_2) \rightarrow (r \cos \phi, r)$ , for  $\phi \rightarrow +\frac{\pi}{2}^-$ ,  $\Delta\lambda \rightarrow 0$  and  $\Delta\phi \rightarrow 0$ , the functions  $\alpha^W$  and  $\alpha^E$  in (14) go to  $-1/2$  while  $\beta^N$  and  $\beta^S$  in (15) go to 0. Hence the limit of matrix  $\mathbf{M}^{-1}\mathbf{A}$  is given by:

$$\mathbf{A}' = \begin{bmatrix} 1 & -1/2 & 0 & \dots & 0 \\ -1/2 & 1 & -1/2 & \ddots & 0 \\ 0 & \ddots & \ddots & \ddots & 0 \\ \vdots & \ddots & \ddots & \ddots & -1/2 \\ 0 & \ddots & \ddots & -1/2 & 1 \end{bmatrix}. \quad (17)$$

The eigenvalues of the matrix in (17) are:

$$\lambda_k = 1 + \cos\left(\frac{k\pi}{n+1}\right) \quad k = 1, \dots, n \quad (18)$$

and then the condition number  $\mu_2(M^{-1}A) = \lambda_{max}/\lambda_{min} \approx n^2/2$  (by using the series expansion of  $\cos x = 1 - x^2/2 + o(x^2)$ ). Moreover for  $\Delta\lambda \rightarrow 0$  and  $\Delta\phi \rightarrow 0$  the size  $n$  of the matrix  $\mathbf{A}$  goes to  $+\infty$  and hence we obtain the thesis. ■

By the proposition (3.1), for  $n$  large and  $\phi \rightarrow \pm\pi/2$ , it is preferable to adopt more suitable preconditioning techniques or a strategy based on the local change of the coordinates at poles. In this paper we propose an alternative approximate sparse inverse preconditioning AINV techniques [7] for the linear system (11). AINV technique is a critical step since the inverse of a sparse matrix is usually dense. The problem is how to build a preconditioner that preserves the sparse structure. We introduce a factored sparse approximate inverse FSAI preconditioner  $\mathbf{P} = \tilde{\mathbf{Z}}\tilde{\mathbf{Z}}^t$  [8, 11], computed by means conjugate-orthogonalization procedure. Specifically, we propose an “ad hoc” method for computing an incomplete factorization of the inverse of the matrix  $\mathbf{T} \subset \mathbf{A}$ , obtained by  $\mathbf{A}$  taking only the elements  $a_{i,j}$  such that  $|j - i| \leq 1$ . The factorized sparse approximate inverse of  $\mathbf{T}$  is used as explicit preconditioner for (11). In the following we give some remarks for the sparsity pattern selection  $S$  of our inverse preconditioner  $\mathbf{P}$ .

**PROPOSITION 3.2** *If  $\mathbf{T}$  is a tridiagonal, symmetric and diagonally dominant matrix, with diagonal elements all positive  $t_{k,k} > 0$ ,  $k = 1, \dots, n$ , then the Cholesky’s factor  $\mathbf{U}$  of the matrix  $\mathbf{T}$  is again diagonally dominant.*

**Proof.** Since  $\mathbf{T}$  is a tridiagonal matrix then  $\mathbf{U}$  is a bidiagonal matrix. Using the inductive method we proof that  $\mathbf{U}$  is diagonally dominant matrix. For  $k = 1$  is trivially, indeed by hypothesis we know that  $|a_{1,1}| > |a_{1,2}| \iff |u_{1,1}^2| > |u_{1,1}u_{1,2}|$ , then we obtain  $|u_{1,1}| > |u_{1,2}|$ . Moreover placed the thesis true for  $k - 1$  i.e.  $|u_{k-1,k-1}| > |u_{k-1,k}|$  then by the following inequalities:

$$\begin{aligned} |a_{k,k}| &> |a_{k,k-1}| + |a_{k,k+1}| \iff \\ |u_{k-1,k}^2 + u_{k,k}^2| &> |u_{k-1,k}u_{k-1,k-1}| + |u_{k,k}u_{k,k+1}| > u_{k-1,k}^2 + |u_{k,k}u_{k,k+1}|. \end{aligned} \quad (19)$$

subtracting the inequality (19) for  $u_{k-1,k}^2$ , then the thesis holds also for  $k$ . ■

This result allows to prove the following proposition:

**PROPOSITION 3.3** *The inverse matrix  $\mathbf{Z}$  of a bidiagonal and diagonally dominant matrix  $\mathbf{U}$  has column vectors  $\mathbf{z}_k, k = 1, \dots, n$  such that starting from diagonal element  $z_{k,k}$ , they contain a finite sequence  $\{z_{k-i,k}\}_{i=0,\dots,k-1}$  strictly decreasing.*

**Proof.** Applying a backward substitution procedure for solving the system of equations  $\mathbf{U}\mathbf{z}_k = \mathbf{e}_k$ , we get:

$$z_{k-i,k} = \begin{cases} 1/u_{k,k} & \text{if } i = 0 \\ (-1)^i / u_{k,k} \cdot \prod_{r=1}^i (u_{k-r,k-r+1} / u_{k-r,k-r}) & \text{if } 0 < i \leq k-1. \end{cases} \quad (20)$$

By means of the preposition (3.2) we obtain that  $z_{k-i,k} > z_{k-i-1,k}$  with  $0 < i \leq k-1$  and hence the thesis is proved. ■

The previous propositions (3.2) and (3.3) enable to select a sparsity pattern  $S$  by the following scheme:

- (1) Consider the symmetric, diagonally dominant and triangular matrix  $\mathbf{T}$ , obtained by  $\mathbf{A}$  taking only the elements  $a_{i,j}$  such that  $|j-i| \leq 1$
- (2)  $\mathbf{T} = \mathbf{U}^T \mathbf{U}$  is diagonally dominant matrix. Consequently its Cholesky factor  $\mathbf{U}$  is diagonally dominant (proposition (3.2)).
- (3)  $\mathbf{U}$  is a bidiagonal and diagonally dominant matrix.  $\mathbf{Z} = \mathbf{U}^{-1}$  has columns vector  $\mathbf{z}_k$ ,  $k = 1, \dots, n$  such that  $z_{k-i,k} > z_{k-i-1,k}$  with  $0 < i \leq k-1$ . (proposition (3.3))
- (4) Fixed an upper bandwidth  $q$ , the entries  $z_{i,j}$  with  $j > i+q$  of  $\mathbf{Z}$  are considered negligible.
- (5) The preconditioner  $\mathbf{P} = \tilde{\mathbf{Z}}\tilde{\mathbf{Z}}^t$  is built as:

$$\tilde{z}_{i,j} = \begin{cases} z_{i,j} & \text{if } j \leq i+q \\ 0 & \text{if } j > i+q \end{cases} \quad (21)$$

- (6) The sparse factor  $\tilde{\mathbf{Z}}$  is computed by  $T$ -orthogonalization procedure posing the sparsity pattern  $S = \{(i,j) / j > i+q\}$

$\mathbf{T}$  is a diagonally dominant matrix then the incomplete inverse factorization of  $\mathbf{T}$  exists for any choice of the sparsity pattern  $S$  on  $\mathbf{Z}$  [8].

From computationally point of view, the  $T$ -orthogonalization procedure with the sparsity pattern  $S$  is based on matrix-vector operations with computational cost of  $5(q+1)$  floating point operations. Moreover, for each column vector  $\tilde{\mathbf{z}}_k$  of  $\tilde{\mathbf{Z}}$  we work only on its  $q+1$  components  $\tilde{z}_k[k-q]$ ,  $\tilde{z}_k[k-q+1]$ , ...,  $\tilde{z}_k[k]$  with consequently global complexity of  $5q(q+1)O(n)$ .

#### 4. Practical Considerations

In this section we give some practical details on the elliptic solver implementation with FSAI preconditioner, on a generic GPU architecture. The matrices  $\mathbf{A}$ ,  $\tilde{\mathbf{Z}}$  and  $\tilde{\mathbf{Z}}^T$  are stored with the special storage format Compressed Sparse Row (CSR). The FSAI is performed in serial on the CPU and its building requires a negligible time on total execution of the elliptic solver. We show the implementation of the Algorithm 1 outlines on the GPUs [12, 13, 20].

---

#### Algorithm 1 FSAI-PCG solver

---

- 1:  $k = 0$ ;  $\mathbf{x}_0 = D_{i,j}^0 = 2D_{i,j}^{t-1}$ , the initial guess;
  - 2:  $\mathbf{r}_0 = \mathbf{b} - \mathbf{A}\mathbf{x}_0$ ;
  - 3:  $\mathbf{s}_0 = \tilde{\mathbf{Z}}\tilde{\mathbf{Z}}^t \mathbf{r}_0$ , with  $\mathbf{P} = \tilde{\mathbf{Z}}\tilde{\mathbf{Z}}^t$  the FSAI preconditioner;
  - 4:  $\mathbf{d}_0 = \mathbf{s}_0$ ;
  - 5: **while** ( $\|\mathbf{r}_k\|/\|\mathbf{b}\| > \epsilon$  .and.  $k \leq n$ ) **do**
  - 6:  $\mathbf{q}_k = \mathbf{A}\mathbf{d}_k$ ;  $\alpha_k = (\mathbf{s}_k, \mathbf{r}_k)/(\mathbf{d}_k, \mathbf{q}_k)$ ;  $\mathbf{x}_{k+1} = \mathbf{x}_k + \alpha_k \mathbf{d}_k$ ;
  - 7:  $\mathbf{r}_{k+1} = \mathbf{r}_k - \alpha_k \mathbf{q}_k$ ;  $\mathbf{s}_{k+1} = \tilde{\mathbf{Z}}\tilde{\mathbf{Z}}^t \mathbf{r}_{k+1}$ ;  $\beta_k = (\mathbf{s}_{k+1}, \mathbf{r}_{k+1})/(\mathbf{s}_k, \mathbf{r}_k)$ ;
  - 8:  $\mathbf{d}_{k+1} = \mathbf{r}_{k+1} + \beta_k \mathbf{d}_k$ ;  $k = k + 1$ ;
  - 9: **end while**
- 

In details, our solver is implemented by means of the CUDA language with the auxiliary linear algebra libraries CUBLAS, for the “dot product” (xDOT), “combined scalar multiplication plus vector addition” (xAXPY), “euclidean norm” (xNRM2) and “vector by a constant scaling” (xSCAL) operations, and CUSPARSE for the sparse matrix-vector operations in the PCG solver. The linear algebra scientific libraries are extremely helpful to easily implement a software on the GPU architecture. A “by-hand” implementation (see Figure 2 and 3) of the solver without the library features is reported as a tedious GPU programming example. In this

```

1 /*GRID and BLOCK CONFIGURATION*/
2 const int warpSize = 32; //Number of threads in a Warp.
3 const int maxGridSize = 65535; //Maximum number of simultaneous Blocks.
4 int warpCount = (n / warpSize) + (((n % warpSize) == 0) ? 0 : 1); //Number of Warps.
5 int threadCountPerBlock = warpSize; //Number of threads per Block.
6 int blockCount = min(maxGridSize, warpCount); //Number of Blocks per kernel.
7 dim3 BlockDim = dim3(threadCountPerBlock, 1, 1); //Set Block dimension.
8 dim3 GridDim = dim3(blockCount, 1, 1); //Set Grid dimension.

```

Figure 2. Grid and block configuration.

```

1 /*MATRIX-VECTOR PRODUCT OF A SPARSE MATRIX IN THE CSR FORMAT*/
2 __global__ void spmv_csr_scalar_kernel(int n, int* start, const int* j,
3 const float* a, const float* d, float* y)
4 {
5     int i = blockDim.x * blockIdx.x + threadIdx.x ;
6     if ( i < n ){
7         int pr1=start[i];
8         int pr2=start[i+1]-1;
9         y[i]=0;
10        for (int q =pr1; q<=pr2; q++)
11            y[i]+=a[q]*d[j[q]];
12    }
13 }
14
15 ...
16
17 int main(int argc, char* argv[]){
18     ...
19     spmv_csr_scalar_kernel<<<GridDim,BlockDim>>>(n,d_start,d_j, d_a ,d_x , d_y);
20     ...
21 }

```

Figure 3. Naive GPU implementation of a function for the matrix-vector product of a matrix in CSR format.

type of coding, the manually configuration of the grid of thread blocks is necessary. For example if we use the TESLA S2050 the variables `warpSize` and `maxGridSize` (respectively at lines 2 and 3) have to be assigned. In details, `warpSize` indicates the number of threads (32) in a warp, which is a sub-division use in the hardware implementation to coalesce memory access and instruction dispatch; `maxGridSize` is the maximum number of simultaneous blocks (65535). Furthermore, `warpCount` (at line 4) represents the number of warps and it depends on the dimension `n` of the problem. In the end, variables `threadCountPerBlock` and `blockCount` (respectively at lines 5 and 6) are the parameter used for setting the grid and block configuration (lines 7 and 8). For example, if `n = 10000` is the size of a vector, then `threadCountPerBlock = 32` and `blockCount = 313`.

The figure 3 shows the matrix-vector product, with the matrix stored in CSR format. We observe that this implementation requires a large amount of kernel functions, invoked by the “host” (CPU) and executed on the “device” (GPU).

In the following, we will show how to implement the Algorithm 1 outlines by using library features. In order to use the CUBLAS library it is necessary initialize it by means of the following instructions:

```

cublasStatus stat;
cublasInit();

```

For the use of the CUSPARSE library two steps are necessary. The first one consists, as follow, in the library initialization:

```

cusparseHandle_t handle=0;
cusparseCreate(&handle);

```

moreover, it is recalled the creation and setup of a matrix descriptor:



```

cusparsMatDescr_t descra=0;
cusparsCreateMatDescr(&descra);
cusparsSetMatType(descra,CUSPARSE_MATRIX_TYPE_GENERAL);
cusparsSetMatIndexBase(descra,CUSPARSE_INDEX_BASE_ZERO);

```

The library avoids to configure the grid of the thread blocks and it allows to write codes in a very fast way. For example, at line 6 of the Algorithm 1 the computation of  $\mathbf{q}_k = \mathbf{A}\mathbf{d}_k$  is required, and this operation can be made simply by calling the CUSPARSE routine `cusparsScsrnv()`, that performs the operation  $\mathbf{q} = a\mathbf{A}\mathbf{d} + b\mathbf{q}$  as follows:

```

cusparsScsrnv(handle, CUSPARSE_OPERATION_NON_TRANSPOSE, n, n,
              a, descra, A, start, j, d, b, q);

```

In our context, `A`, `j` and `start` represent the symmetric positive-definite matrix  $\mathbf{A}$ , stored in the CSR format. More precisely, the vector `A` denotes the non-zero elements of the matrix  $\mathbf{A}$ , `j` is the vector that stores the column indexes of the non-zero elements, the vector `start` denotes, for each row of the matrix, the address of the first non-zero element and `n` represents the row and columns number of the square matrix  $\mathbf{A}$ . The constants `a` and `b` are assigned to 1.0 and 0.0 respectively. Moreover it happens that at line 6 of the Algorithm 1, the computation of  $(\mathbf{s}_k, \mathbf{r}_k)$  is performed by means the CUBLAS routine for the dot product:

```

alfa_num = cublasSdot(n, s, INCREMENT_S, r, INCREMENT_R);

```

The constants `INCREMENT_S` and `INCREMENT_R` are both assigned to 1. Last operation of line 6 in Algorithm 1, is the  $\mathbf{x}_{k+1} = \mathbf{x}_k + \alpha_k \mathbf{d}_k$  for updating the solution and it is implemented by calling the CUBLAS routine for the saxpy operation:

```

cublasSaxpy(n, alfa, d, INCREMENT_D, x, INCREMENT_X);

```

The constants `INCREMENT_D` and `INCREMENT_X` are both assigned to 1. In addition, the computation of  $\mathbf{s}_{k+1} = \tilde{\mathbf{Z}}\tilde{\mathbf{Z}}^t\mathbf{r}_{k+1}$  at line 7 is the preconditioning step of the linear system (11) and it is computed by means of two matrix-vector operations performed as:

```

cusparsScsrnv(handle, CUSPARSE_OPERATION_NON_TRANSPOSE, n, n,
              a, descra, Z_t, start_Z_t, j_Z_t, r, b, zt);
cusparsScsrnv(handle, CUSPARSE_OPERATION_NON_TRANSPOSE, n, n,
              a, descra, Z_t, start_Z, j_Z, zt, b, z);

```

In details, in the first call of `cusparsScsrnv()`,  $\mathbf{z}t = \tilde{\mathbf{Z}}^t\mathbf{r}_{k+1}$  and  $\mathbf{s}_{k+1} = \tilde{\mathbf{Z}}\mathbf{z}t$  are computed. We have outlined just few of computational operations because the other will be performed in the same way. The parameters `handle`, `CUSPARSE_OPERATION_NON_TRANSPOSE` and `descra` are discussed in the NVIDIA report [17] in more detailed way. In summary, we highlight how the use of the standard library, designed for the GPU architecture, allow to optimize the computational oceanographic simulation model.

Matrix Name	Size	Matrix non-zeros elements
ORCA-2	$180 \times 149$	133800
ORCA-05	$751 \times 510$	1837528
ORCA-025	$1442 \times 1021$	7359366

Table 1. NEMO-OPA grid resolutions.

<b>A</b> Dimension	$\mathbf{P}$ ( $\phi \approx 0$ )	$\mathbf{P}^{-1}$ ( $\phi \approx 0$ )	$\mathbf{P}$ ( $\phi \approx \pi/2$ )	$\mathbf{P}^{-1}$ ( $\phi \approx \pi/2$ )
ORCA-2	271	460	8725	26820
ORCA-05	1128	1593	22447	86280
ORCA-025	2458	3066	28513	139742

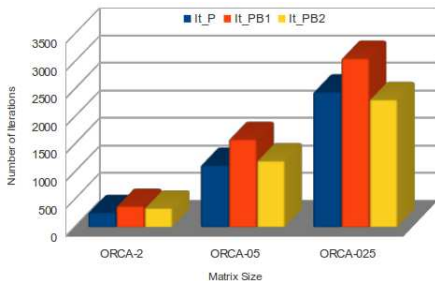
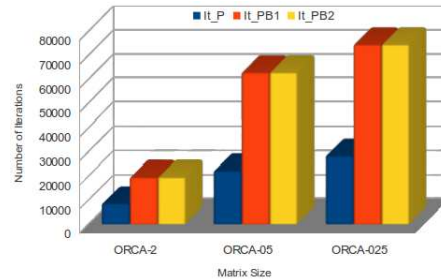
Table 2. Comparison between  $\mathbf{P}$  and  $\mathbf{P}^{-1}$  in terms of Number of Iterations of the PCG in the case  $\mathbf{A}$  is well-conditioned ( $\phi \approx 0$ ) and  $\mathbf{A}$  ill-conditioned ( $\phi \approx \pi/2$ ), varying the problem dimensions.

## 5. Numerical Experiments

In this section we focus on the important numerical issues of our elliptic solver implemented with GPU architecture in single precision. The solver is tested on three grid size resolutions of the NEMO-OPA ocean model (Table 1).

In the Table 2, we compare the performance in terms of PCG iterations of the proposed inverse bandwidth preconditioner  $\mathbf{P}$  respect to  $\mathbf{P}^{-1}$ , that is the diagonal NEMO-OPA preconditioner. We fix an accuracy of  $\epsilon = 10^{-6}$  on the relative residue  $r = \|\mathbf{Ax} - \mathbf{b}\|/\|\mathbf{b}\|$  on the linear system solution. The experiments are carried out in the case of well-conditioned  $\mathbf{A}$  matrix, corresponding to the geographical case of  $\phi \approx 0$  and in the case of ill-conditioned  $\mathbf{A}$  with  $\phi \approx \pi/2$ . We can observe as in the worst case with  $n$  large and  $\mathbf{A}$  ill-conditioned the PCG with  $\mathbf{P}^{-1}$  has a very slow convergence with a huge number of iterations to reach the fixed accuracy. The experiment, reported in the Table 2, highlights the poor performance of the  $\mathbf{P}^{-1}$  for solving the Laplace elliptic problem (11) within OPA-NEMO.

In the following, we show the performance in terms of PCG iterations of  $\mathbf{P}$  respect to the AINV Bridson Class preconditioners, that believe to CUSP library. To be more specific, let us consider the  $\mathbf{P}_{B1}$  and  $\mathbf{P}_{B2}$  Bridson's preconditioners, obtained by means of the  $A$ -orthogonalization method. The first is given by posing a (fixed) drop tolerance and by ignoring the elements below the fixed tolerance [9] and in the second one is predetermined the number of non-zeros elements on each its row. [10].

Figure 4. Comparison between  $\mathbf{P}$ ,  $\mathbf{P}_{B1}$  and  $\mathbf{P}_{B2}$  in terms of Number of Iterations of the PCG ( $y$ -axis) when  $\mathbf{A}$  is well-conditioned, varying the problem dimensions ( $x$ -axis)Figure 5. Comparison between  $\mathbf{P}$ ,  $\mathbf{P}_{B1}$  and  $\mathbf{P}_{B2}$  in terms of Number of Iterations of the PCG ( $y$ -axis) when  $\mathbf{A}$  is ill-conditioned, varying the problem dimensions ( $x$ -axis)

The required accuracy on the solution is fixed to  $\epsilon = 10^{-6}$  on the relative residue. In Figure 4 we report the PCG iterations of  $\mathbf{P}$ ,  $\mathbf{P}_{B1}$  and  $\mathbf{P}_{B2}$  in the case of the matrix

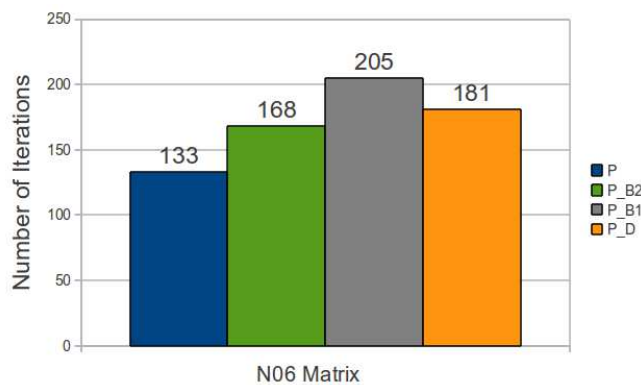


Figure 6. PCG iterations.  $\mathbf{P}$  is the proposed preconditioner,  $\mathbf{P}_d$  is  $\mathbf{P}^{-1}$ ,  $\mathbf{P}_{B1}$   $\mathbf{P}_{B2}$  are  $\mathbf{P}_{B1}$  and  $\mathbf{P}_{B2}$

Matrix Name	Non-zeros Elem.	Mem. Occ.
ORCA-2	133800	4MB
ORCA-05	1837528	37MB
ORCA-025	7359366	135MB

Table 3. Matrix memory occupancy. Mem Occ. is the full memory allocated memory on the GPU.

$\mathbf{A}$  well-conditioned ( $\phi \approx 0$ ). In Figure 5 we present the case of the ill-conditioned ( $\phi \approx \pi/2$ ) matrix  $\mathbf{A}$ . The numerical results show as the number of iterations of the solver  $\mathbf{P}$  is comparable to  $\mathbf{P}_{B1}$  and  $\mathbf{P}_{B2}$  when the dimensions of the problem are small or middle. Furthermore, it is strongly indicated to use  $\mathbf{P}$  with a huge problem dimension. We test  $\mathbf{P}$ ,  $\mathbf{P}^{-1}$ ,  $\mathbf{P}_{B1}$  and  $\mathbf{P}_{B2}$  on the sparse matrix N0S6 of the Market Matrix database [22] by setting the required accuracy on the computed solution to  $\epsilon = 10^{-6}$  and the band  $q$  of the preconditioner to 4. This sparse matrix is obtained in the Lanczos algorithm with partial re-orthogonalization Finite difference approximation to Poisson’s equation in an L-shaped region, mixed boundary conditions.

The figure 6 shows as  $\mathbf{P}$  achieves the best performance in terms of iterations. Finally, we test the elliptic solver implementation on GPU architecture. The numerical experiments are carried out on an “NVIDIA TESLA S2050” card, based on the “FERMI GPU”. The “TESLA S2050” consists of 4 GPGPUs, each of which with 3GB of RAM memory and 448 processing cores working at 1.55 GHz. All runs are given on 1 GPU device. We have adopted CUDA release 4.0, provided by NVIDIA as a GPGPU environment and the numerical code is implemented by using the single precision arithmetic.

As described in the previous sections by using scientific computing library it is not necessary manually setting up the block and grid configuration on the memory device. The number of blocks required to store the elliptic solver input data (in CSR format) do not have to exceed the maximum sizes of each dimension of a GPU grid device. Schematic results of GPU memory utilization for ocean model resolutions are presented in the Table 3. Observe that in our numerical experiments we do not fill the memory of the TESLA GPU and the simulations run also on cheaper or older boards, as for example the Quadro 4700FX. Generally, it is possible to grow the grid dimensions of the ocean model according to the memory capacity of the available GPU.

The elliptic solver requires a large amount of Sparse-Matrix Vector (`cusparsCsrnv`) multiplications, vector reductions and other vector operation to be performed. CPU version is implemented in ANSI C executed in serial on a

2.4GHz “Intel Xeon E5620” CPU, with 12MB of cache memory. Serial and GPU versions are in single precision. We test the performance of the solver in terms of Floating Point Operations (FLOPS). The performance of the numerical experiments (reported in the Figure 8) are given in the case of  $A$  ill-conditioned matrix ( $\phi \approx \pi/2$ ). We count an average of the iterations of solver and the complexity of all linear algebra operations involved in both serial and parallel implementations. The “GPU solver” (blue) and “CPU solver” (orange) curves represent the GFLOPS of the solver, respectively, for the CPU and GPU versions.

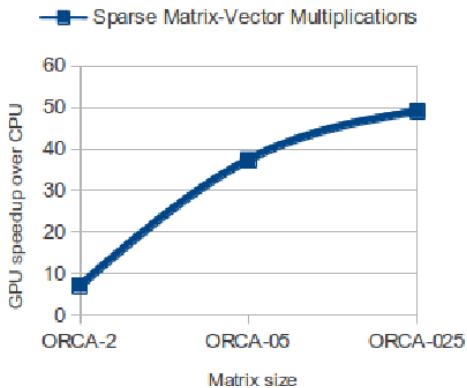


Figure 7. Sparse-Matrix Vector multiplications speed-up.

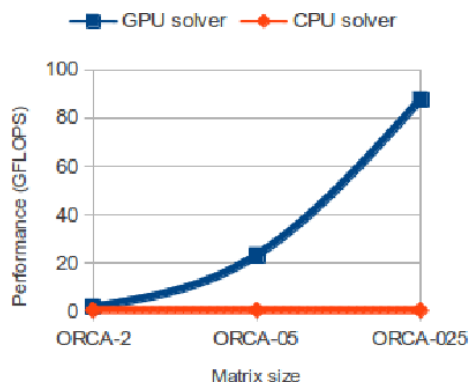


Figure 8. CPU and GPU comparison of the solver in terms of GFLOPS.

The main recalled computational kernels in the solver are the Sparse-Matrix Vector. From the Figure 7 we highlight the improvement in terms of GFLOPS speed-up by replacing `gemv()` with `cusparseCsrmmv()` function. These results prove that, increasing the model grid resolution, it is possible to exploit the computational power of the GPUs. In details, the GPU solver implementation in the ORCA-025 configuration has a peak performance of 87 GFLOPS respect to 1,43 GFLOPS of the CPU version.

## 6. Conclusions

The ocean modelling is a challenging application where expensive computational kernels are fundamental tools to investigate the physics of the ocean and the climate change. In a lot of applications, the elliptic Laplace equations are used in the complex mathematical models; they represents critical computational points since the convergence of the numerical solvers to a solution, within a reasonable number of iterations, it is not always guaranteed. In our case, this happens to the preconditioning technique of the OPA-NEMO ocean model, for which we prove to be inefficient and inaccurate. In this paper, we have proposed a new inverse preconditioner based on the FSAI method that shows better results respect to the OPA-NEMO diagonal one and to others of the Bridson class. Moreover, an important contribute is given by an innovative approach for parallelizing the elliptic solver on the Graphical Processing Units (GPU) by means of the scientific computing libraries. The library based implementation of the computing codes allows to optimize oceanic framework reducing the simulation times and to develop computational solvers easy-to-implement.

## 7. Acknowledgments

The computing resources and the related technical support used for this work have been provided by CRESCO/ENEAGRID “High Performance Computing infrastructure” and its staff with particular acknowledgments to the researcher Marta Chinnici; CRESCO/ENEAGRID is funded by ENEA, the “Italian National Agency for New Technologies, Energy and Sustainable Economic Development” and by national and European research programs. See [www.cresco.enea.it](http://www.cresco.enea.it) for more information.

## References

- [1] Rouillet, G. and G. Madec., *Salt conservation, free surface, and varying levels : a new formulation for ocean general circulation models*, J. Geophys. Res, 105, 2000.
- [2] Gries M., Boning C., Bryan F.O., et al. *Developments in ocean climate modeling*, Ocean modeling Volume 2.
- [3] Madec G, *NEMO-OPA ocean engine*, Institute Pierre-Simon Laplace (IPSL), France, 2012.
- [4] Higdon R. *Numerical modeling of ocean circulation*, Acta Numerica, Cambridge University Press.
- [5] Epicoco I., S. Mocavero, E. Scoccimarro and G. Aloisio. *ORCA025: Performance Analysis on Scalar Architecture*, CMCC Research Paper N. 50.
- [6] Arakawa A., F. Mesinger, *Numerical Methods used in Atmospheric Models*, VOL 1 Garp Publication Series NO 17, France (1976).
- [7] Benzi M., *Preconditioning techniques for large linear systems: A survey*, J. Comput. Phys., 182, 2002.
- [8] Benzi M., C. D. Meyer, and M. Tuma, *A sparse approximate inverse preconditioner for the conjugate gradient method.*, SIAM J. Sci. Comput. 17, 1995.
- [9] Bridson R. and W.-P. Tang, *Refining an approximate inverse*, J. Comput. Appl. Math. 22, 2000.
- [10] Lin C.J. and J. J. More, *Incomplete Cholesky factorizations with limited memory*, SIAM J.Sci. Comput., 21, 1999.
- [11] Benzi M. *An explicit preconditioner for the conjugate gradient method* Proceedings of the Cornelius Lanczos International Centenary Conference, J. D. Brown et al., eds., Society of Industrial and Applied Mathematics, Philadelphia.
- [12] Bell N. and M. Garland, *Efficient sparse matrix-vector multiplication on CUDA*, NVIDIA Technical Report NVR-2008-004, NVIDIA Corporation, 2008.
- [13] Farina R., S. Cuomo and P. De Michele, *A CUBLAS-CUDA Implementation of PCG Method of an Ocean Circulation Model*, AIP Conf. Proc. September 14, Volume 1389, 2011.
- [14] Dongarra J. et al., *Templates for the Solution of Linear Systems: Building Blocks for Iterative Methods, 2nd Edition*, SIAM, Philadelphia, PA, 1994.
- [15] NVIDIA, *NVIDIA CUDA programming guide* <http://developer.download.nvidia.com>, Nvidia Technical Report, 2012.
- [16] NVIDIA, *CUBLAS Library*, <http://developer.download.nvidia.com>, Nvidia Technical Report, 2007.
- [17] NVIDIA, *CUSPARSE Library*, <http://developer.download.nvidia.com>, Nvidia Technical Report, 2012.
- [18] *Cusp Library*, <http://code.google.com/p/cusp-library/>.
- [19] Farina R., S. Cuomo and P. De Michele *An Inverse Preconditioner for a Free Surface Ocean Circulation Model*, submitted to AIP Conf. Proc. July 10, 2012.
- [20] Farina R., S. Cuomo, P. De Michele and M. Chinnici. *Inverse Preconditioning Techniques on a GPUs Architecture in Global Ocean Models*, Euro Siam proceedings 2011.
- [21] Duff I.S., A.M. Erisman, C.W. Gear, and J.K. Reid, *Sparsity structure and Gaussian elimination*, *SIGNUM Newsl.* 23, 2 (1988).
- [22] Market Matrix web site, <http://math.nist.gov/MatrixMarket/data/Harwell-Boeing/lanpro/nos6.html> (2012).
- [23] Dukowicz, J.K., Smith, R.D., Malone, R.C., *A reformulation and implementation of the Bryan Cox Semtner ocean model on the connection machine*, Journal of Atmospheric and Oceanic Technology 10, 195-208.
- [24] Webb, D.J., 1996. *An ocean model code for array processor computers*. Computers and Geophysics 22.
- [25] Webb, D.J., Coward, A.C., de Cuevas, B.A., Gwilliam, C.S., 1997. *A multiprocessor ocean general circulation model using message passing*. Journal of Atmospheric and Oceanic Technology 14.